Materials Research Bulletin 129 (2020) 110906

Contents lists available at ScienceDirect

Materials Research Bulletin

journal homepage: www.elsevier.com/locate/matresbu

Vapor growth of Bi_2Se_3 and Bi_2O_2Se crystals on mica

K.A. Kokh[a,b,*], N.A. Nebogatikova[b,c], I.V. Antonova[b,c,d], D.A. Kustov[c], V.A. Golyashov[c], E.S. Goldyreva[a,b], N.P. Stepina[c], V.V. Kirienko[c], O.E. Tereshchenko[b,c]

[a] Sobolev Institute of geology and mineralogy SB RAS, Novosibirsk, 630090, Russia
[b] Novosibirsk State University, Novosibirsk, 630090, Russia
[c] Rzhanov Institute of Semiconductor Physics SB RAS, Novosibirsk, 630090, Russia
[d] Novosibirsk State Technical University, Novosibirsk, 630087, Russia

ARTICLE INFO

Keywords:
Physical vapor deposition
Bismuth selenide
Epitaxy
Mica
Electrical properties
Microstructure

ABSTRACT

Thin Bi_2Se_3 films were deposited on mica substrates by physical vapor deposition without the use of the carrier gas. It was found that the films with high structural quality and high conductivity are grown at a source temperature of approximately 500 °C. The resistance of 20–300 nm thick films is in the range of 10^2-10^4 Ω/sq as compared with ~10 Ω/sq for thicker films. Bi_2O_2Se crystals with a similar resistivity are revealed to grow at higher temperatures (600–700 °C). It was suggested that the decrease of the thin film resistance is due to the contribution of the surface channels. Low resistivity of the Bi_2Se_3 films expands the scope of their possible applications as infra-red transparent electrodes.

1. Introduction

The discovery of topological insulators (TIs) is a recent breakthrough in the field of condensed matter. TIs have been at the forefront of material research due to their unique electronic properties and potential for a wide range of applications. The surface states of a three-dimensional (3D) topological insulator are composed of two-dimensional gapless Dirac cones, which have a helical spin structure in a momentum space [1,2]. A typical representative of this class is Bi_2Se_3, which has a good chemical stability [3,4], relatively large bandgap (~0.3 eV), and the n-type bulk conductivity $n \sim 10^{19}$ cm^{-3}. Bi_2Se_3 demonstrates the properties of the topological insulator at relatively high temperatures [5,6]. It is a layered compound consisting of 1 nm thick packages of weakly coupled quintets (Se-Bi-Se-Bi-Se) and having an anisotropic resistance ($\rho_{zz}/\rho_{xx} \sim 10$) [7].

In thin films (less than 100 nm thick), the volume conductivity can be reduced and a conductive channel formed at the surface with the same spin orientation of electrons [8,9] begins to prevail in their conductivity. Recent results on thin film growth have shown the prospects of their use for the creation of vertical van-der-Waals heterostructures with other 2D materials [10]. However, the existing methods for the preparation of bismuth chalcogenide samples have shown that due to the fragility of this material, thin films obtained by mechanical, liquid-phase or electrochemical stratification are usually limited in size to several tens of microns [8,9,11,12]. Layered Bi_2O_2Se has aroused increasingly widespread interest because of its high carrier mobility (comparable to that in graphene), air-stability, quasi-two dimension nature, and size-tunable bandgap [13]. As a result, Bi_2O_2Se nanosheets have a great potential for their future applications in ultrafast, flexible, and low power electronic and optical devices [14]. These novel materials and related hybrid structures are expected to serve as a platform for the development of future electronic devices. The growth from the gas phase resulted in significant progress in the lateral size of the films. The molecular beam epitaxy (MBE) technique implies an ultra-high vacuum, allows controlling the growth on the atomic layer, and provides the growth of Bi_2Se_3 on many substrates, even having a large lattice mismatch [15–17]. But MBE is extremely expensive compared to the alternative chemical vapor deposition (CVD) method, which operates at conventional fore vacuum pump pressures. In this method, due to evaporation in the hot zone, Bi_2Se_3 material is condensed on the substrates located in colder parts of the reactor [18,19]. In addition to the charge and substrate temperature, a significant contribution to the transfer process is provided by the introduction of carrier gas into the system, the flow rate of which is an important parameter [20].

The aim of this work is to analyze the epitaxial vapor growth of Bi_2Se_3 films on mica substrates without the use of carrier gas at different temperatures and durations of the process. As a result, the optimal growth regime for Bi_2Se_3 films with high structural quality and high conductivity is found to carry out at source temperature T_s = 500 °C. Bi_2O_2Se crystals are revealed to grow at higher

* Corresponding author at: Sobolev Institute of geology and mineralogy SB RAS, Novosibirsk, 630090, Russia.
E-mail address: kokh@igm.nsc.ru (K.A. Kokh).

https://doi.org/10.1016/j.materresbull.2020.110906
Received 1 October 2019; Received in revised form 24 March 2020; Accepted 20 April 2020
Available online 25 April 2020

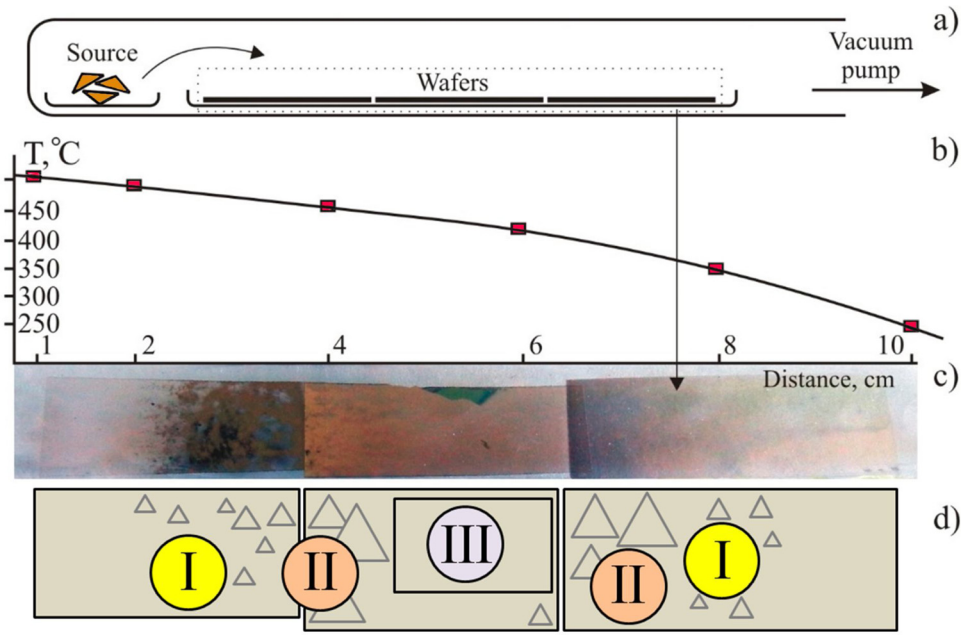

Fig. 1. (a) Scheme of the growth reactor; (b) Temperature distribution inside the empty reactor at the source temperature T_s = 500 °C; (c) Photo of the mica substrates after the Bi_2Se_3 deposition at T_s = 500 °C; (d) A typical result of deposition obtained for T_s below 550 °C: I is the zone of oxidized Bi_2Se_3 islands, II is the transition zone, and III is the zone of Bi_2Se_3 film.

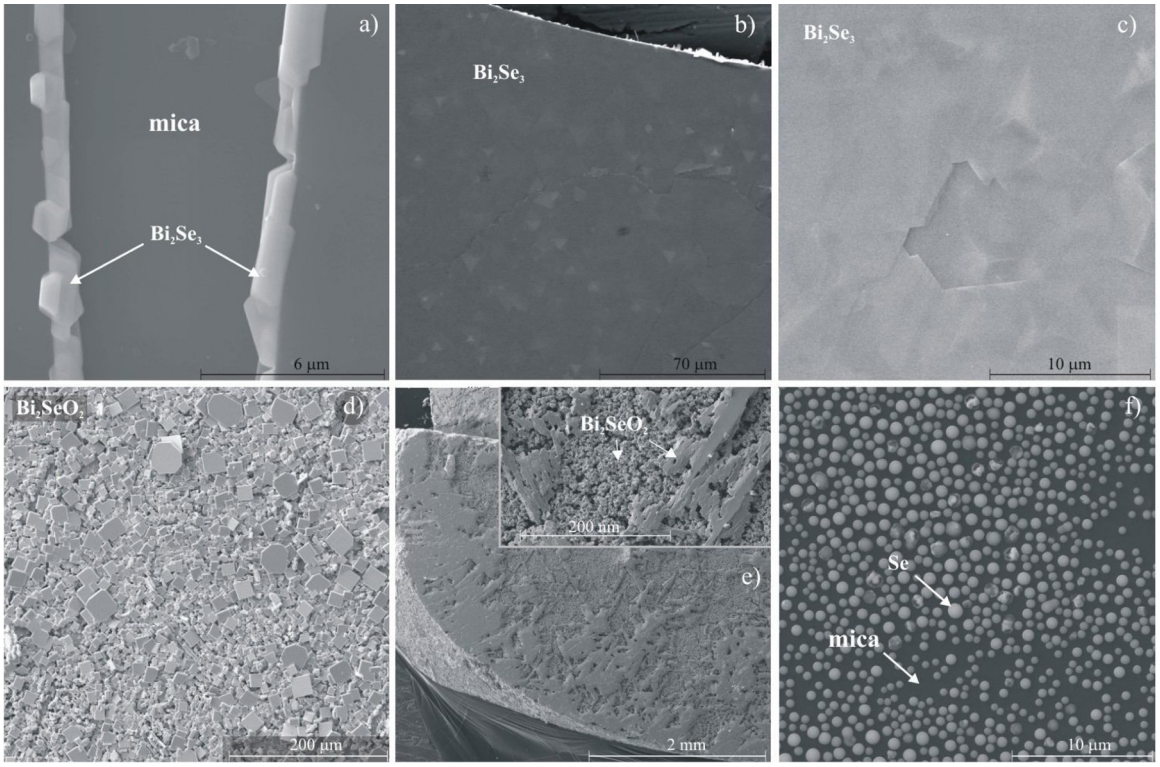

Fig. 2. SEM images of the samples obtained at different T_s: (a) initial stage of the Bi_2Se_3 growth on mica steps (T_s = 400 °C); (b) Bi_2Se_3 layer in zone III (T_s = 500 °C, 8 h of deposition); (c) thick Bi_2Se_3 layer after 20 h of the deposition at T_s = 500 °C; (d) formation of the Bi_2O_2Se phase on the mica substrate and (e) on the source surface at $T_s \geq 600$ °C; and (f) selenium particles on the cold part of the substrate grown at $T_s \geq 600$ °C.

temperatures (600–700 °C).

2. Experimental

A scheme of the PVD reactor is shown in Fig. 1a. The quartz glass ampoule with a sealed end is placed in a horizontal heating furnace. The opposite end is at room temperature and is connected to the fore vacuum pump. There are two holders inside the reactor. The first one with a piece of Bi_2Se_3 single crystal is placed in a high temperature part of the reactor. The second holder containing the substrates for growth is located in the part with some temperature gradient. Measurements carried out in an empty reactor demonstrate a temperature drop of ~250°C along the place for substrates (Fig. 1b). Strips of cleaved along (001) mica about 10 mm × 40 mm in size were taken as the substrates (Fig. 1c). Before loading into the reactor, the surface layer of mica was removed by scotch. The experiments were conducted at the source temperatures in the range of 400–700 °C. After pumping the reactor the furnace was turned on for heating at 200 °C/hour rate. The samples

were cooled in the reactor with the furnace switched off. The total growth time varied in the range of 4.5–22 hours.

The structure, surface morphology and thickness of grown films were analyzed using an atomic force microscope (AFM) Solver PRO NT-MDT in contact or semi-contact modes. The X-ray diffraction pattern from the substrate surface was obtained by the arlx'TRA POWbyDER analyzer (CuKα radiation). The Tescan Mira 3 LMU scanning electron microscope (SEM) with an EDX analyzer was used to study the film morphology and composition. The Raman spectra excited by 532 nm radiation were obtained by a Horiba JobinYvonLabRAM HR800 spectrometer with an LN/CCD detector. The film conductivity at room temperature was studied using a 4-probe JANDEL head and HM21 analyzer. The electrical measurements of conductivity on individual crystallites at room temperature were carried out using a Keithley 6485 picoammeter with contacts made from conductive silver paste. The temperature dependence of conductivity was measured by the two- or four-terminal method with Keithley electrometers. The temperature stability was controlled using a Ge thermometer.

3. Results and discussion

After the deposition process at $T_s > 400$ °C, the central part of all substrates had a uniform metallic luster (Fig. 1c). According to SEM, part of the film nearest to the source is nonuniform and the film growth starts with the nucleation on the substrate steps (Fig. 2a). It is suggested that these islands are the oxidized Bi_2Se_3 film nucleus (*see* Raman data and Fig. 3). The next region includes a continuous Bi_2Se_3 film. The length of region II depended on the process time and source temperature. SEM analysis shows that the film morphology is a homogeneous coating with triangular hills oriented in two directions (Fig. 2b). The EDX spectrum was not reliable showing many impurities such as Al, O, Si, and Mg originated from mica. The unalloyed chemical composition of $Bi_{2.085}Se_{2.925}$ was measured on a thick layer obtained by a long deposition (more than 20 h) at $T_s = 500$ °C (Fig. 2c). For the growth at $T_s \geq 600$ °C the films consist of the layer of tabular crystals up to 80 microns in size (Fig. 2d). According to the EDX data, the phase of such crystals is bismuth oxyselenide Bi_2O_2Se, a layered semiconductor with promising electronic properties [21,22]. Most likely, the partial oxidation of Bi_2Se_3 to Bi_2O_2Se occurs due to oxygen formed from the thermal decomposition of mica. The formation of the new phase is also observed on the surface of Bi_2Se_3 source crystal (Fig. 2e). It is interesting to note the presence of elementary selenium globules on the cold part of the substrates (Fig. 2f).

Raman spectroscopy provides additional data, using which we identified deposited products in the different zones of samples. The material spectrum in the middle of the zone III well corresponds to the peaks of the bulk Bi_2Se_3 (Fig. 3a, b). Small deviation in modes position in the Raman spectra is most likely associated with weak variation in the film stoichiometry or defect concentrations. Similar variations in the positions of E_g^2 and A_{1g}^2 modes are also observed in the bulk crystals [23,24]. The length of zone III depends on the source temperature and process duration. Zone III is surrounded by zone II, which were indistinguishable in SEM. The Raman spectra for the thin film from zone II has the spectrum generally similar to Bi_2Se_3 but with a weak additional peak at 260 cm^{-1} (Fig. 3c), which is interpreted as the presence of BiO_x phase in combination with the high-quality Bi_2Se_3 film [25]. On the other hand, the spectra from zone I had the only peak at 260 cm^{-1}, which most likely corresponds to the oxidation of the grown islands after the exposition of the sample to the air (see Fig. 3d). Thus, it may be concluded that the absence of oxide traces in region III as shown by the Raman spectra indicates the high structural quality and oxidation resistance of the Bi_2Se_3 material.

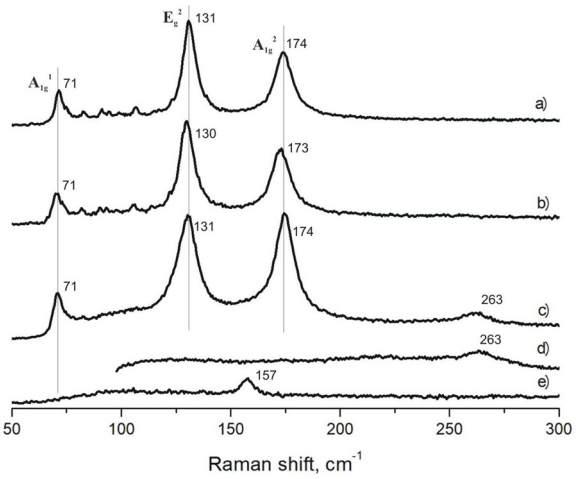

Fig. 3. Raman spectra: for bulk Bi_2Se_3(a); deposited film from zone III (b) and II (c) ($T_s = 500$ °C, 8 h of deposition); (d) fully oxidized film from zone I obtained after 4.5 h of deposition at $T_s = 500$ °C; and (e) tabular crystals of Bi_2O_2Se.

The tabular crystals obtained at $T_s = 600$ and $T_s = 700$ °C have a single Raman peak at 160 cm^{-1} (Fig. 3e), which correlates with the spectrum of Bi_2O_2Se, given in [26].

AFM images of the deposited layer grown for 14 h at $T_s = 500$ °C are given in Fig. 4. In zone I (first 1–3 cm from the source) there are individual crystallites of 5–20 microns in lateral size and thicknesses of 4 and 8 nm (Fig. 4a, b). The angles between the layer edges are 60 or 120 degrees reflecting the trigonal symmetry of Bi_2Se_3. Zone II contains a continuous film of crystallites with the step height of 4 nm (Fig. 4c). The film thickness in this zone is varied from 20 to 400 nm. The central part of substrate corresponds to zone III where the surface becomes smoother (Fig. 4d). Here the step height of 1 nm is sometimes observed that corresponds to the thickness of 1 quintuple layer (Se-Bi-Se-Bi-Se). In the case of lower source temperature $T_s = 450$ °C, the growth slows down significantly. The grain size reaches 300–500 nm, and the relief is several nanometers. At $T_s = 400$ °C no traces of new phase were found.

The growth at higher temperatures ($T_s = 550$ °C) results in the formation of films consisting of individual particles of 100–300 nm in size and 30–60 nm in thickness. A further increase of source temperature (600–700 °C) leads to a strong relief on the film surface.

The results of X-ray diffraction are shown in Fig. 5. The presence of (00X) reflexes of the Bi_2Se_3 phase and absence of any extra peaks associated with the oxide phase for all samples grown at the source temperature up to 550 °C confirms the implementation of Van der Waals epitaxy between Bi_2Se_3 and mica. The Bi_2O_2Se phase appears in a case of films formed at $T_s > 550$ °C.

The grown film resistance was studied with the use of the four-probe head (the Kelvin technique) at room temperature. Generally, it was found that the continuous film in zones II and III has a relatively low sheet resistivity, whereas samples from zone I are non-conductive. The results for the films grown at $T_s = 500$ °C and at different durations are presented in Fig. 6. It is well known that the film resistance strongly depends on the thickness of Bi_2Se_3 films. Decrease in film thickness leads to strong increase in this resistance from 10^{-3} to 10^{-4} Ω/sq for bulk crystals to 8–80 kΩ/sq for nanometer thickness of the film [27]. It is worth noting the gradual increase in resistance while substrates move away from the source. We associate this effect with a decrease in the film thickness. However, the decrease in the growth time does not affect the resistance of films obtained at the beginning of zone III. These films are characterized by the resistance value 10^2–10^4 Ω/sq, with resistance falling down to ~50 Ω/sq for relatively long growth time. An increase of the source temperature to more than 500 °C leads to a decrease in region length of the conductive part of the film due to the Bi_2O_2Se phase formation. Low resistance films could be applied as transparent electrodes for the IR range where Bi_2Se_3 has very low absorption [28].

The grown films were compared with that obtained by the exfoliation from a bulk Bi_2Se_3 crystal. It was found that the exfoliated film resistivity was 10^3–10^4 Ω/sq and independent on their thickness if less

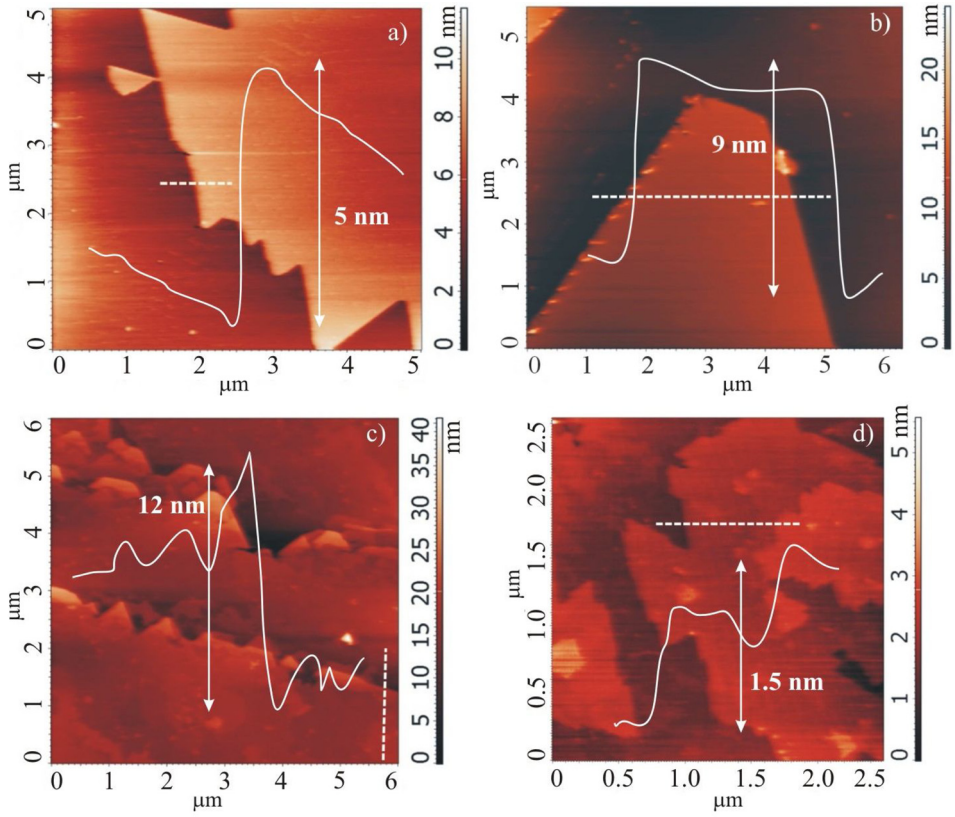

Fig. 4. AFM images and typical profile of the film grown at T_s = 500 °C during 14 h: (a, b) – Zone I, individual crystallites; (c) Zone II, rough layer; and (d) Zone III, continuous smooth film. The solid line shows the depth profile along the dashed line.

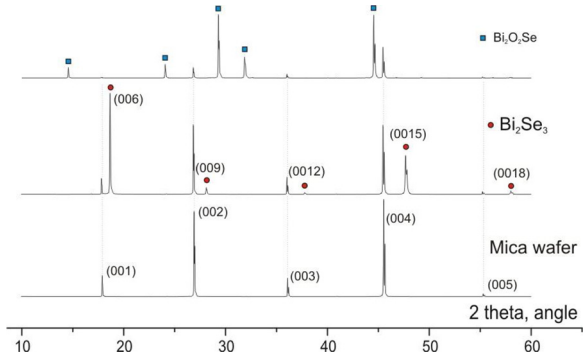

Fig. 5. X-ray diffraction patterns from the mica wafer, the Bi_2Se_3 film from zone III grown at $T_s \leq$ 550 °C, and the Bi_2O_2Se phase obtained at T_s ~600-700 °C.

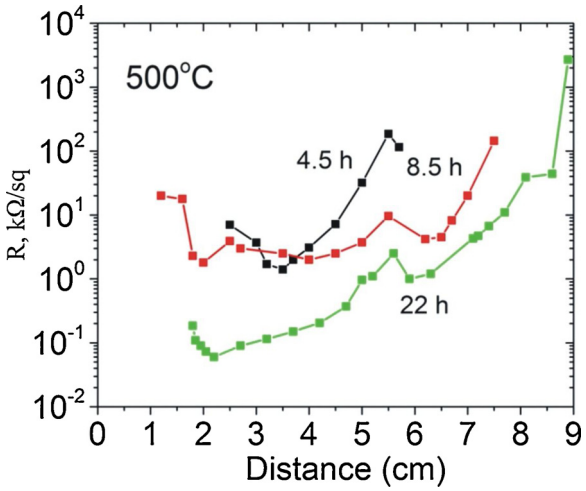

Fig. 6. The electrical resistance of Bi_2Se_3 films grown at the source temperature of T_s = 500 °C at different growth times.

than 80 nm. Similar effect was observed for $BiSbTeSe_2$ films with a thickness less than 100 nm [29]. We guess that constant value of resistance is determined by the surface Bi_2Se_3 channels, while smaller resistance values measured for thicker samples can be due to the contribution of bulk Bi_2Se_3.

To understand the mechanism of conductivity, we compare the temperature dependence of resistance R(T) for grown Bi_2Se_3 film and bulk Bi_2Se_3 crystal (Fig. 7). The bulk sample demonstrates the metallic-like temperature dependence with a weakly changeable electron concentration in the range of $n \sim (1 \div 3) \times 10^{19}\,cm^{-3}$ measured in the 4.2–300 K temperature range (Fig. 7a). For the epitaxially grown film Bi_2Se_3film from zone III (Fig. 7b) there are three main temperature regions in R(T) dependence that is in agreement with Ref. [30]. At temperatures above 27 K, the conductivity is determined by the electron-phonon interaction. In the temperature range of 7–27 K, G(T) = 1/R(T) is described by the logarithmic dependence characteristic for the weak localization regime or two-dimensional electron-electron interaction [31]. The R(T) behavior in the low-temperature range (below 7 K) can be due to the influence of defects or transition to the weak anti-localization, which is often observed in such films with a decrease in the temperature [29].

4. Conclusions

In our experiments, there was a gradient of temperature along the substrates. The phase composition of the deposited type of material was strongly dependent on the temperature and distance from the source. If the temperature was too high (600 °C or higher), the Bi_2Se_3 reacted

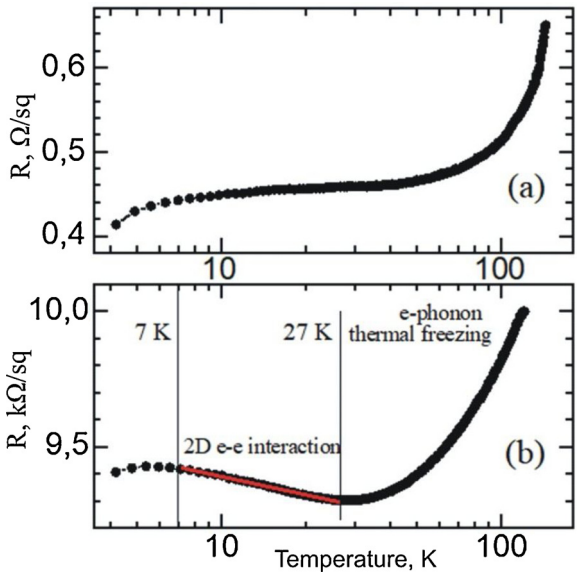

Fig. 7. Temperature dependences of the resistance for (a) bulk Bi_2Se_3; for Bi_2Se_3 film from zone III (b).

with mica producing Bi_2O_2Se. At lower temperatures, Bi_2Se_3 dominates in the intermediated part and forms the films with relatively large length.

The van-der-Waals epitaxy of Bi_2Se_3 on the mica substrate is most effectively realized at the source temperature of 500 °C. The variation of growth conditions (source temperatures, growth time, and vapor pressure) efficiently tunes the film thickness. The main part of the deposited layer is characterized by high structural properties and low resistivity. The resistance of the films with a 20–300 nm thickness is in the range of 10^2-10^4 Ω/sq and independent on film thickness that can be explained by the determining contribution of the surface channels. The resistance of the thicker films can reach a value down to ~50 Ω/sq. Such properties expand the scope of their possible applications. In addition to the expected applications in spintronics, the films could be applied as electrodes transparent in the IR range.

Author credit statement

K.A. Kokh: manuscript writing, crystal growth experiments
E.S. Goldyreva: crystal growth experiments
N.A.Nebogatikova: AFM analysis
I.V. Antonova, D.A. Kustov, N.P. Stepina, V.V. Kirienko: resistivity measurements
V.A. Golyashov: Raman, x-ray analyses
O.E.Tereshchenko: project supervision

Declaration of Competing Interest

The authors declare no conflict of interests

Acknowledgments

This study was supported by RFBR 18-29-12094, Russian Science Foundation (17-12-01047), Saint Petersburg State University (Grant ID 40990069) and state assignment of IGM SB RAS.

References

[1] S.I. Vedeneev, Quantum oscillations in three-dimensional topological insulators, PhysicsUspekhi 60 (4) (2017) 385–401.
[2] H.J. Zhang, C.X. Liu, X.L. Qi, X. Dai, Z. Fang, S.C. Zhang, Topological insulators in Bi_2Se_3, Bi_2Te_3 and Sb_2Te_3 with a single Dirac cone on the surface, Nat. Phys. 5 (6) (2009) 438442.
[3] V.A. Golyashov, K.A. Kokh, S.V. Makarenko, K.N. Romanyuk, I.P. Prosvirin, A.V. Kalinkin, O.E. Tereshchenko, A.S. Kozhukhov, D.V. Sheglov, S.V. Eremeev, S.D. Borisova, E.V. Chulkov, Inertness and degradation of (0001) surface of Bi_2Se_3 topological insulator, J. Appl. Phys. 112 (11) (2012) 113702.
[4] O.E. Tereshchenko, K.A. Kokh, V.V. Atuchin, K.N. Romanyuk, S.V. Makarenko, V.A. Golyashov, A.S. Kozhukhov, I.P. Prosvirin, A.A. Shklyaev, Stability of the (0001) surface of the Bi_2Se_3 topological insulator, JETP Lett. 94 (6) (2011) 465–468.
[5] S.Z. Butler, S.M. Hollen, L.Y. Cao, Y. Cui, J.A. Gupta, H.R. Gutierrez, T.F. Heinz, S.S. Hong, J.X. Huang, A.F. Ismach, E. Johnston-Halperin, M. Kuno, V.V. Plashnitsa, R.D. Robinson, R.S. Ruoff, S. Salahuddin, J. Shan, L. Shi, M.G. Spencer, M. Terrones, W. Windl, J.E. Goldberger, Progress, challenges, and opportunities in two-dimensional materials beyond graphene, ACS Nano 7 (4) (2013) 2898–2926.
[6] D. Hsieh, Y. Xia, D. Qian, L. Wray, J.H. Dil, F. Meier, J. Osterwalder, L. Patthey, J.G. Checkelsky, N.P. Ong, A.V. Fedorov, H. Lin, A. Bansil, D. Grauer, Y.S. Hor, R.J. Cava, M.Z. Hasan, A tunable topological insulator in the spin helical Dirac transport regime, Nature 460 (7259) (2009) 1101–U59.
[7] H. Kőhler, C.R. Becker, Optically active lattice vibrations in Bi_2Se_3, Phys. Status Solidi B 61 (1974) 533–537.
[8] D.L. Mo, W.B. Wang, Q. Cai, Influence of thickness on the electrical transport properties of exfoliated Bi_2Te_3 ultrathin films, Nanoscale Res. Lett. 11 (2016) 354.
[9] N. Bansal, Y.S. Kim, M. Brahlek, E. Edrey, S. Oh, Thickness-independent transport channels in topological insulator Bi_2Se_3 thin films, Phys. Rev. Lett. 109 (11) (2012) 116804.
[10] S.G. Xu, Y. Han, X.L. Chen, Z.F. Wu, L. Wang, T.Y. Han, W.G. Ye, H.H. Lu, G. Long, Y.Y. Wu, J.X.Z. Lin, Y. Cai, K.M. Ho, Y.H. He, N. Wang, van der Waals epitaxial growth of atomically thin Bi_2Se_3 and thickness-dependent topological phase transition, Nano Lett. 15 (4) (2015) 2645–2651.
[11] L.P. Sun, Z.Q. Lin, J. Peng, J. Weng, Y.Z. Huang, Z.Q. Luo, Preparation of few-layer bismuth selenide by liquid-phase-exfoliation and its optical absorption properties, Sci. Rep. 4 (2014) 4794.
[12] O. Chiatti, C. Riha, D. Lawrenz, M. Busch, S. Dusari, J. Sanchez-Barriga, A. Mogilatenko, L.V. Yashina, S. Valencia, A.A. Unal, O. Rader, S.F. Fischer, 2D layered transport properties from topological insulator Bi_2Se_3 single crystals and micro flakes, Sci. Rep. 6 (2016) 27483.
[13] C. Chen, M.X. Wang, J.X. Wu, H.X. Fu, H.F. Yang, Z. Tian, T. Tu, H. Peng, Y. Sun, X. Xu, J. Jiang, N.B.M. Schroter, Y.W. Li, D. Pei, S. Liu, S.A. Ekahana, H.T. Yuan, J.M. Xue, G. Li, J.F. Jia, Z.K. Liu, B.H. Yan, H.L. Peng, Y.L. Chen, Electronic structures and unusually robust bandgap in an ultrahigh-mobility layered oxide semiconductor, Bi_2O_2Se, Sci. Adv. 4 (9) (2018) eaat8355.
[14] J. Li, Z.X. Wang, Y. Wen, J.W. Chu, L. Yin, R.Q. Cheng, L. Lei, P. He, C. Jiang, L.P. Feng, J. He, High-performance near-infrared photodetector based on ultrathin Bi_2O_2Se nanosheets, Adv. Funct. Mater. 28 (10) (2018) 1706437.
[15] M. Vyshnepolsky, C. Klein, F. Klasing, A. Hanisch-Blicharski, M. Horn-von Hoegen, Epitaxial growth of the topological insulator Bi_2Se_3 on Si(111): growth mode, lattice parameter, and strain state, Appl. Phys. Lett. 103 (11) (2013) 111909.
[16] X.Y. Liu, D.J. Smith, H.L. Cao, Y.P. Chen, J. Fan, Y.H. Zhang, R.E. Pimpinella, M. Dobrowolska, J.K. Furdyna, Characterization of $Bi2Te_3$ and $Bi2Se_3$ topological insulators grown by MBE on (001) GaAs substrates, J. Vacuum Sci. Technol. B 30 (2) (2012) 02B103.
[17] S. Schreyeck, N.V. Tarakina, G. Karczewski, C. Schumacher, T. Borzenko, C. Brune, H. Buhmann, C. Gould, K. Brunner, L.W. Molenkamp, Molecular beam epitaxy of high structural quality Bi_2Se_3 on lattice matched InP(111) substrates, Appl. Phys. Lett. 102 (4) (2013) 041914.
[18] Y.C. Lin, Y.S. Chen, C.C. Lee, J.K. Wu, H.Y. Lee, C.T. Liang, Y.H. Chang, A study on the epitaxial Bi_2Se_3 thin film grown by vapor phase epitaxy, AIP Adv. 6 (6) (2016) 065218.
[19] W.S. Zheng, T. Xie, Y. Zhou, Y.L. Chen, W. Jiang, S.L. Zhao, J.X. Wu, Y.M. Jing, Y. Wu, G.C. Chen, Y.F. Guo, J.B. Yin, S.Y. Huang, H.Q. Xu, Z.F. Liu, H.L. Peng, Patterning two dimensional chalcogenide crystals of Bi_2Se_3 and In_2Se_3 and efficient photodetectors, Nat. Commun. 6 (2015) 6972.
[20] P. Gu, J.L. Yu, X.L. Zeng, S.Y. Cheng, Y.F. Lai, H.F. Zhou, Q. Zheng, Effect of temperature and gas flow on Bi_2Se_3 nanoplates grown by chemical vapor deposition, J. Nanosci. Nanotechnol. 18 (11) (2018) 7590–7594.
[21] J.X. Wu, H.T. Yuan, M.M. Meng, C. Chen, Y. Sun, Z.Y. Chen, W.H. Dang, C.W. Tan, Y.J. Liu, J.B. Yin, Y.B. Zhou, S.Y. Huang, H.Q. Xu, Y. Cui, H.Y. Hwang, Z.F. Liu, Y.L. Chen, B.H. Yan, H.L. Peng, High electron mobility and quantum oscillations in non-encapsulated ultrathin semiconducting Bi_2O_2Se, Nat. Nanotechnol. 12 (6) (2017) 530–534.
[22] M.M. Meng, S.Y. Huang, C.W. Tan, J.X. Wu, Y.M. Jing, H.L. Peng, H.Q. Xu, Strong spinorbit interaction and magnetotransport in semiconductor Bi_2O_2Se nanoplates, Nanoscale 10 (6) (2018) 2704–2710.
[23] W. Richter, H. Kohler, C.R. Becker, Raman and far-Infrared investigations of phonons in rhombohedral V2-VI3 compounds ? Bi2Te3, Bi2Se3, Sb2Te3, and Bi2(Te1-xSex)3 (0 < x < 1), Bi1-ySby)2Te3 (0 < y < 1), Phys. Status Solidi B Basic Res. 84 (2) (1977) 619–628.
[24] I. Childres, J.F. Tian, I. Miotkowski, Y. Chen, AFM and Raman studies of topological insulator materials subject to argon plasma etching, Philos. Mag. 93 (6) (2013) 681–689.
[25] J. Zhang, C. Yang, M. Liu, S. Jiang, C. Zhang, Z. Sun, F. Liu, Y. Xu, B. Man, Fabrication of graphene/ Bi_2Se_3 /graphene heterostructure without the surface oxidation of Bi_2Se_3, Front. Nansci. Nanotech. 1 (1) (2015) 19–22.
[26] T. Cheng, C.W. Tan, S.Q. Zhang, T. Tu, H.L. Peng, Z.R. Liu, Raman spectra and strain effects in bismuth oxychalcogenides, J. Phys. Chem. C 122 (34) (2018) 1997019980.

[27] I.V. Antonova, N.A. Nebogatikova, K.A. Kokh, D.A. Kustov, R.A. Soots, A.V. Golyashov, O.E. Tereshchenko, Electrochemically exfoliated thin Bi2Se3 films and van der Waals heterostructures Bi2Se3/graphene, Nanotechnology 31 (2020) 125602.

[28] H.L. Peng, W.H. Dang, J. Cao, Y.L. Chen, W. Wu, W.S. Zheng, H. Li, Z.X. Shen, Z.F. Liu, Topological insulator nanostructures for near-infrared transparent flexible electrodes, Nat. Chem. 4 (4) (2012) 281–286.

[29] Y. Xu, I. Miotkowski, C. Liu, J.F. Tian, H. Nam, N. Alidoust, J.N. Hu, C.K. Shih, M.Z. Hasan, Y.P. Chen, Observation of topological surface state quantum hall effect in an intrinsic threedimensional topological insulator, Nat. Phys. 10 (12) (2014) 956–963.

[30] J. Chae, S.H. Kang, S.H. Park, H. Park, K. Jeong, T.H. Kim, S.B. Hong, K.S. Kim, Y.K. Kwon, J.W. Kim, M.H. Cho, Closing the surface bandgap in thin Bi_2Se_3 /graphene heterostructures, ACS Nano 13 (4) (2019) 3931–3939.

[31] A.M. Shikin, I.I. Klimovskikh, S.V. Eremeev, A.A. Rybkina, M.V. Rusinova, A.G. Rybkin, E.V. Zhizhin, J. Sanchez-Barriga, A. Varykhalov, I.P. Rusinov, E.V. Chulkov, K.A. Kokh, V.A. Golyashov, V. Kamyshlov, O.E. Tereshchenko, Electronic and spin structure of the topological insulator $Bi_2Te_{2.4}$ $Se_{0.6}$, Phys. Rev. B 89 (12) (2014) 125416.